Mon. Not. R. Astron. Soc. **000**, 000–000 (0000) Printed 2 February 2008 (MN LATEX style file v2.2)

arXiv:0711.3607v1 [astro-ph] 22 Nov 2007

Star formation, metallicity gradient and ionized gas: clues to the formation of the elliptical galaxies NGC 6868 and NGC 5903

M.G. Rickes[1], M.G. Pastoriza[1] and C. Bonatto[1]
[1] *Departamento de Astronomia, Universidade Federal do Rio Grande do Sul, Av. Bento Gonçalves 9500, Porto Alegre, RS, Brazil.*

2 February 2008

ABSTRACT

The stellar population, metallicity distribution and ionized gas in the elliptical galaxies NGC 6868 and NGC 5903 are investigated in this paper by means of long-slit spectroscopy and stellar population synthesis. Lick indices in both galaxies present a negative gradient indicating an overabundance of Fe, Mg, Na and TiO in the central parts with respect to the external regions. We found that Mg_2 correlates both with $\mathrm{FeI}_{\lambda 5270}$ and $\mathrm{FeI}_{\lambda 5335}$, suggesting that these elements probably underwent the same enrichment process in NGC 6868. However, only a marginal correlation of Mg_2 and $\mathrm{FeI}_{\lambda 5270}$ occurs in NGC 5903. The lack of correlation between computed galaxy mass and the Mg_2 gradient suggests that these elliptical galaxies were formed by merger events. The stellar population synthesis shows the presence of at least two populations with ages of 13 Gyr and 5 Gyr old in both galaxies.

We have estimated the metallicity of the galaxies using SSP models. The central region of NGC 6868 ($|R| \lesssim 0.5$ kpc) presents a deficiency of alpha elements with respect to iron and solar metallicity. The external parts, present a roughly uniform distribution of [α/Fe] ratios and metallicities ranging from $[Z/Z_\odot] = -0.33$ and solar. A similar conclusion applies to NGC 5903.

Concerning the emitting gas conspicuously detected in NGC 6868, we test three hypotheses as ionizing source: an H II region, post-AGB stars and an Active Galactic Nucleus (AGN). Diagnostic diagrams involving the ratios $[NII]_{\lambda 6584}/H\alpha$, $[OI]_{\lambda 6300}/H\alpha$ and $[SII]_{\lambda 6717,31}/H\alpha$, indicate that values measured in the central region of NGC 6868 are typical of LINERs. Together with the stellar population synthesis, this result suggests that the main source of gas ionization in NGC 6868 is non-thermal, produced by a low-luminosity AGN, probably with some contribution of shocks to explain ionization at distances of ~ 3.5 kpc from the nucleus.

Key words: Elliptical galaxies: NGC 6868 and NGC 5903 - fundamentals parameters

1 INTRODUCTION

A question still open to debate is how elliptical galaxies are formed. Three scenarios have been proposed to address this issue: *(i)* monolithic collapse of gas clouds linked to high energy dissipation rates (Arimoto & Yoshii 1987); *(ii)* galaxy merger (Burkert & Naab 2000); and *(iii)* hybrid models that involve an early monolithic collapse followed by merger events at later times (Ogando et al. 2005). A consequence of the monolithic collapse (associated to a large-scale star formation) is that a conspicuous metallicity gradient is expected to establish along the full range of galactic radius (e.g. Carollo et al. 1993a; Chiosi & Carraro 2002). However, if merger events are important, the gradient is expected to disappear. A few ellipticals present strong signs of recent dynamical perturbation (Schweizer et al. 1990), which may provide important clues to their formation processes and evolution.

Important information on the above issues has been derived from metal line-strength indices (e.g. Davis et al. 1987) and their radial variation within galaxies. $Mg2$ line-strength distribution in early-type galaxies, for example, can vary considerably, ranging from essentially featureless to structured profiles showing, e.g., changes of slope possibly associated with kinematically decoupled cores, or anomalies in the stellar population of some ellipticals (Carollo et al. 1993b).

In addition, the origin of the ionized gas in ellipticals is another controversial issue, because until recently it was believed that the interstellar medium (ISM) in these galaxies was not significant. However, studies by, e.g. Phillips et al. (1986) have shown that more than 50% of the elliptical and lenticular galaxies contain significant amounts of ionized gas. More recently, Macchetto et al. (1996) have traced ionized gas in a sample of 73 elliptical and SO galaxies by means of narrow-band filters centered on Hα and [NII]. They detected emission gas in about 3/4 of the galaxies, with masses amounting to 10^3 to $10^5\,M_\odot$.

In the present work we investigate properties of the elliptical galaxies NGC 6868 and NGC 5903, because previous studies have shown that they contain important interstellar medium (Macchetto et al. 1996; Ferrari et al. 1999), have complex stellar and gas kinematics (Caon et al. 2000). Besides, both ellipticals belong to galaxy groups, which might imply past close encounters (and even mergers) with companions. Potential consequences of such past interactions are the triggering of discrete star formation events with stellar populations differing in metallicity and age (Worthey et al. 1992) and the presence of large-scale dynamical perturbations that may affect galaxy morphology by building subsystems such as a stellar and/or dust disk (Caon et al. 2000). In this context, NGC 6868 and NGC 5903 can be taken as interesting candidates where the stellar population and metallicity distribution can be investigated, which are important parameters to understand the formation and evolution of these galaxies.

The main goal of the present paper is to investigate, by means of long-slit spectroscopy, the origin, star-formation history, metallicity and ionized gas distribution in NGC 6868 and NGC 5903. The analyses will be based mostly on a stellar population synthesis method (based on templates built with star clusters and H II regions), and the radial distribution of absorption and emission lines.

This paper is organized as follows. In Sect. 2 we describe the observations. Lick indices are measuremed are discussed in Sect. 3. The stellar population synthesis and results are described in Sect. 4. Metallicity and ionized gas are discussed in Sect. 5. Discussions are in Sect. 6.

2 THE TARGET GALAXIES AND SPECTROSCOPIC OBSERVATIONS

NGC 6868 is classified as E3 in RC3[1]. It is part of the GR28 cluster which contains as well the galaxies NGC 6861, NGC 6870, NGC 6851 and NGC 6861D (Maia et al. 1989). Figure 1 shows an R band image of the field containing NGC 6868 in two scales (obtained from the NASA/IPAC Extragalactic Database - NED).

The effective radius of NGC 6868 is $Re = 40''$ (Carollo et al. 1993a). NGC 6868 is a radio source (Savage et al. 1977) and emits in the infrared as indicated by 60 and 100 μm IRAS observations. The total luminosity in the medium infrared is $15.2 \times 10^8\,L_\odot$, and the dust mass estimated from grain emission considerations is $\approx 70\,M_\odot$ (Ferrari et al. 2002).

The velocity field and velocity dispersion profiles are symmetrical about the galaxy center. However, the gas is not observed to follow regular orbits (Zeilinger et al. 1996). The latter work shows evidence in several position angles that the rotation curve does not remain flat in the outer parts but bends back towards a value close to the systemic velocity.

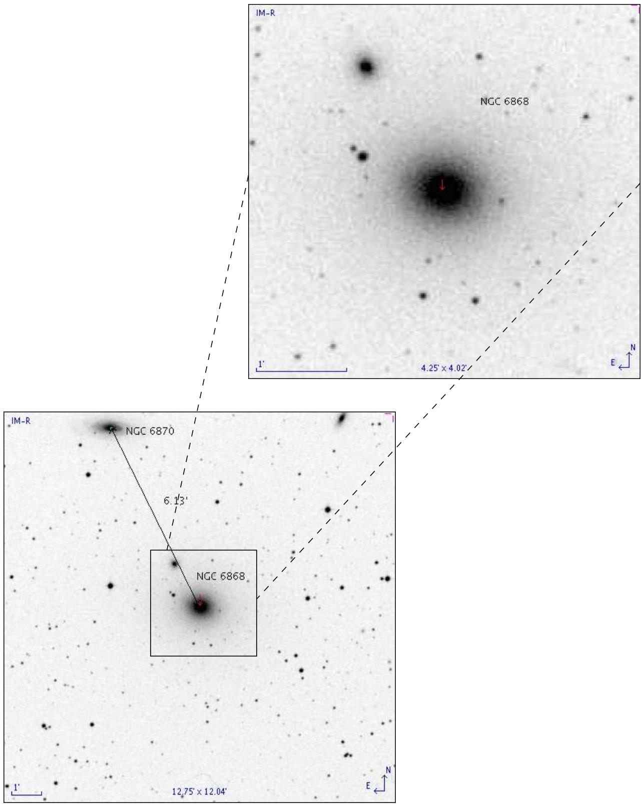

Figure 1. Bottom panel: R image of NGC 6868 showing a scale of $12.75' \times 12.04'$. Top panel: same as before for the region $4.25' \times 4.02'$ centered on NGC 6868.

NGC 5903 (morphological type E2 - RC3) forms a pair with the elliptical galaxy NGC 5898; both galaxies are the brightest members of a small group composed of NGC 5903, NGC 5898 and ESO 514-G 003 (Maia et al. 1989). NGC 5903 presents a small rotation around the semi-major axis (Sparks et al. 1985). Dust is observed in a small region ($\sim$ 100 pc) (Ferrari et al. 1999). NGC 5903 presents X-ray emission with no evidence of ionized gas (O'Sullivan et al. 2001). The effective radius of NGC 5903 is $Re = 37''$ (Carollo et al. 1993a). B images (from NED) of the field containing NGC 5903 are shown in Fig. 2.

NGC 6868 and NGC 5903 were observed with the 3.6 m ESO telescope (in Chile) equipped with EFOSC1. The observational setup included the grism 0150 for the range 5140 to 6900 Å, with a dispersion of 3.4 Å pixel^{-1}, and the CCD#2 (512 × 512 Tektronix). This setup was used in order to maximize the spectral coverage $\Delta\lambda\,5100 - 6800$Å and obtain the largest possible number of stellar absorption features and gas emission lines without compromising the spectral resolution of 3.4Å pixel^{-1} (Caon et al. 2000). The spatial scale of the observational setup was $0.6''$ pixel^{-1} with a $3.1'$ long slit; the slit width was fixed at $1.5''$, approximately equal to the seeing.

---

[1] The Third Reference Catalogue of bright galaxies (de Vaucouleurs et al. 1991).

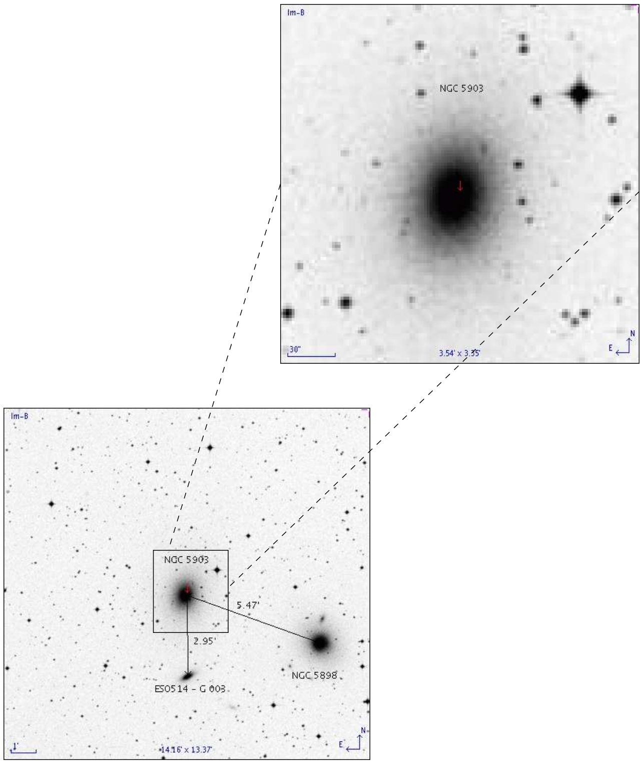

Figure 2. Bottom panel: B image of the field of NGC 5903 showing a scale of $14.16' \times 13.37'$. Top panel: same as before for the region $3.54' \times 3.35'$ centered on NGC 5903.

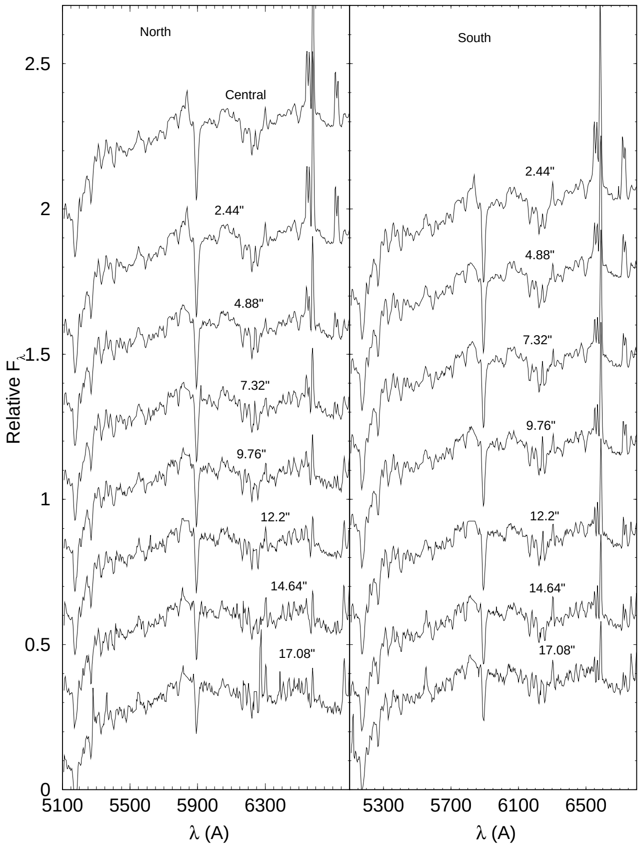

Figure 3. Rest-frame spectra extracted from NGC 6868, corrected for foreground reddening. The distance of each extraction to the galaxy center is given in arcsec. North and south extractions are shown in the left and right panels, respectively. Arbitrary constants have been added to the spectra for clarity. Conspicuous emission lines (especially H_α and [NII]$\lambda\lambda$6548, 6584) occur in all spectra.

At least two spectra were obtained along the position angle in order to increase the signal-to-noise ratio and for cosmic ray removal. For NGC 6868 three long-slit spectra were obtained with 40 min of exposure time; the slit was oriented along the semi-major axis (PA = 120°). Two 40 min spectra were obtained for NGC 5903 with the slit oriented along the semi-major axis (PA = 340°). The seeing varied from $1.2''$ to $1.8''$. Several spectrophotometric standard stars were observed at the beginning and end of each night in order to flux calibrate the spectra. The spectra were processed with standard IRAF tasks. The mean bias was subtracted from each spectra, which were subsequently divided by a normalized dome flat-field to remove variations in sensitivity. The centroids of the non-saturated lines in the He+A comparison spectra were measured in order to obtain the wavelength calibration and to map the line curvature. Galaxy and standard stars spectra were rectified and rebinned to a logarithmic scale with a constant step of $85\,\mathrm{km\,s^{-1}}$. The sky contribution for each galaxy spectra was determined by taking the median value between two windows of 20 pixels wide at both ends of the slit and subtracted.

Spectra were extracted in both galaxies for the central and 7 regions symmetrically distributed along the north-south direction. Pairs of spectra obtained at the same distance of the galaxy center were averaged together in order to increase the signal to noise ratio. We have estimated in less than 1% the relative spectrophotometric errors between both extractions at each position. The distance of each extraction to galaxy center is given in cols. 1 to 3 of Table 2, respectively in terms of angular, effective and absolute radii. For redshift correction we used the conspicuous absorption line NaI_{5895} as reference. Foreground reddening was corrected assuming the Galactic extinction law of Cardelli et al. (1989), with $A_V = 0.085$ (NGC 6868) and $A_V = 0.332$ (NGC 5903) using the $E(B-V)$ values taken from NED and assuming $A_V = 3E(B-V)$. The spectra of NGC 6868 and NGC 5903, corrected for redshift and foreground reddening, are shown in Figs. 3 and 4, respectively. The distances of NGC 6868 and NGC 5903, computed assuming the Hubble constant $\mathrm{H_O} = 75\,\mathrm{km\,s^{-1}}$, are 38 Mpc and 34 Mpc respectively. Accordingly, one arcsec is equivalent to 184 pc for NGC 6868 and 164 pc for NGC 5903.

3 LICK INDICES

NGC 6868 and NGC 5903 present strong absorption lines of neutral iron and sodium, as well as Mg2 and TiO bands in their visible spectra (Figs. 3 and 4) that, together with the continuum distribution, can be used to estimate the age and metallicity of the stellar population. In the present work we adopt the Lick system (Faber et al. 1985; Worthey 1994) to measure equivalent widths (EWs) for the absorption features Mg$_2$ λ5176, Fe$I_{\lambda5270}$, Fe$I_{\lambda5335}$,

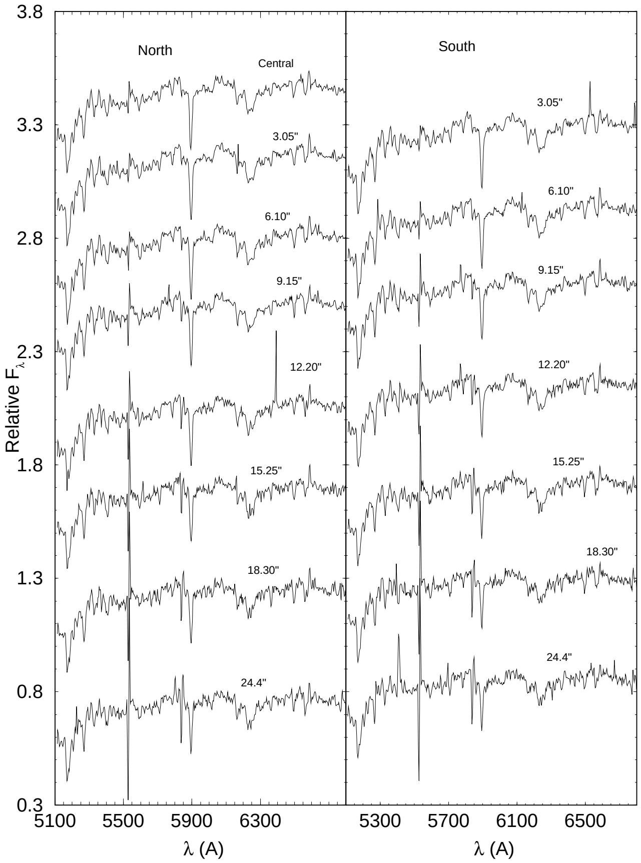

Figure 4. Same as Fig. 3 for NGC 5903.

Table 1. Correction factors $C(\sigma)$

NGC 6868								
λ(Å)	$0''$	$2.4''$	$4.8''$	$7.3''$	$9.7''$	$12.2''$	$14.6''$	$17.08''$
5176	1.21	1.22	1.21	1.21	1.21	1.21	1.21	1.24
5270	1.10	1.12	1.11	1.11	1.11	1.11	1.10	1.13
5335	1.22	1.26	1.23	1.23	1.23	1.23	1.26	1.27
5406	1.20	1.23	1.24	1.24	1.24	1.24	1.23	1.24
5709	1.13	1.16	1.15	1.15	1.15	1.15	1.16	1.18
5782	1.18	1.18	1.18	1.18	1.18	1.18	1.18	1.25
5895	1.09	1.10	1.09	1.10	1.10	1.10	1.10	1.09
6237	1.08	1.08	1.08	1.08	1.08	1.08	1.08	1.09
NGC 5903								
λ(Å)	$0''$	$3.05''$	$6.10''$	$9.15''$	$12.20''$	$15.25''$	$18.30''$	$24.40''$
5176	1.07	1.08	1.06	1.05	1.05	1.05	1.05	1.08
5270	1.10	1.09	1.07	1.08	1.08	1.08	1.08	1.09
5335	1.26	1.25	1.21	1.21	1.21	1.21	1.21	1.25
5406	1.36	1.29	1.30	1.30	1.30	1.30	1.30	1.29
5709	1.40	1.35	1.37	1.37	1.37	1.37	1.37	1.35
5782	1.45	1.45	1.32	1.28	1.28	1.28	1.28	1.45
5895	1.06	1.04	1.03	1.03	1.03	1.03	1.03	1.03
6237	1.14	1.13	1.12	1.12	1.12	1.12	1.12	1.13

FeI$_{\lambda5406}$, FeI$_{\lambda5709}$, FeI$_{\lambda5782}$, NaI$_{\lambda5895}$ and Tio$_{\lambda6237}$. Continuum values, normalized at λ5870Å, were measured at λ5300, 5546, 5650, 5800, 6173, 6620, and 6640 Å. The velocity dispersion in NGC 6868 varies from $\sim 260 \pm 20\,\mathrm{km\,s^{-1}}$ in the center to $\sim 220 \pm 30\,\mathrm{km\,s^{-1}}$ in the external regions and from $\sim 240 \pm 20\,\mathrm{km\,s^{-1}}$ in the center to $\sim 200 \pm 40\,\mathrm{km\,s^{-1}}$ in the external regions of NGC 5903 (Caon et al. 2000). Therefore, the observed EW values were corrected for line broadening due to stellar velocity dispersion. The spectrum of the G giant star HR 5333, assumed to have zero intrinsic velocity, was broadened with a series of Gaussian filters with velocity dispersion σ varying from 0 to $300\,\mathrm{km\,s^{-1}}$ in steps of $10\,\mathrm{km\,s^{-1}}$.

For each absorption feature considered we calculate an empirical correction index C(σ), so that $C(\sigma)_{Mg2} = \frac{Mg2(0)}{Mg2(\sigma)}$, and $C(\sigma)_{FeI} = \frac{W_\lambda(0)}{W_\lambda(\sigma)}$. We calculate the correction index $C(\sigma)$ for each extracted spectrum using the σ values given by Caon et al. (2000). The resulting correction factors, computed for each feature in all extractions, for both galaxies are given in Table 1. EWs measured in the spectra of NGC 6868 and NGC 5903 are given in Table 2. Except for EW(Mg$_2$ λ5176), which is measured in magnitude, the remaining EWs are given in Å (e.g. Rickes et al. 2004). Different values of EWs are computed allowing for three choices of the continuum level around a given feature, which basically reflect the subjectiveness associated to continuum determination. EWs given in Table 2 correspond to the average values obtained from this process; the uncertainties correspond to the respective standard deviation.

The radial dependence of the EWs are shown in Figs. 5 and 6, respectively for NGC 6868 and NGC 5903. Indices of NGC 6868 consistently present a negative gradient (Fig. 5) that indicates an overabundance of Fe, Mg, Na and TiO in the central parts with respect to the external regions.

A conspicuous negative gradient of the indices Mg$_2$ λ5176, FeI$_{\lambda5270}$, FeI$_{\lambda5335}$, NIa$_{\lambda5895}$ and TiO$_{\lambda6237}$ is observed in NGC 5903 (Fig. 6).

As shown in Fig. 7, Mg_2 correlates both with FeI$_{\lambda5270}$ and FeI$_{\lambda5335}$, which suggests that these elements probably underwent the same enrichment process in NGC 6868. However, only a marginal correlation of Mg_2 and FeI$_{\lambda5270}$ occurs in NGC 5903.

If the galaxy gravitational potential is strong enough to retain the gas ejected by stars and supernovae, it eventually migrates to the galaxy's central regions. New generations of stars will be more metal rich at the center than in the external parts, and a steep radial negative metallicity gradient is established as a mass-dependent parameter. Thus, a galaxy formed essentially through a monolithic collapse is expected to present well-defined correlations between metallicity gradients and mass (Carollo et al. 1993a; Ogando et al. 2005).

Carollo et al. (1993a) investigated the correlation of the gradient $d\mathrm{Mg}_2/dlog\,r$ with galaxy mass for a sample of 42 elliptical galaxies, including NGC 6868 and NGC 5903. They found that the Mg_2 gradient presents a bimodal trend with mass, in the sense that for galaxy mass smaller than $\sim 10^{11} M_\odot$, the gradient increases with mass. No pattern in the gradient was observed for larger masses. The increase in the Mg_2 gradient with mass was interpreted as the result of a dissipative collapse associated with star formation at

Table 2. Equivalent widths measured in the spectra of NGC 6868 and NGC 5903

$R('')$	R/R_e	$R(kpc)$	EW (mag)	EW (Å)						
			$\mathrm{Mg}_2$5176	FeI5270	FeI5335	FeI5406	FeI5709	FeI5782	NaI5895	TiO6237
NGC 6868										
0.00	0.00	0.00	0.27 ± 0.01	3.71 ± 0.09	3.34 ± 0.05	2.54 ± 0.01	1.23 ± 0.02	1.26 ± 0.02	5.51 ± 0.02	5.78 ± 0.13
2.44S	0.06	0.46	0.25 ± 0.01	3.53 ± 0.38	3.12 ± 0.16	2.36 ± 0.12	1.20 ± 0.05	1.29 ± 0.03	5.43 ± 0.02	5.78 ± 0.12
4.88S	0.12	0.92	0.23 ± 0.01	3.29 ± 0.23	3.21 ± 0.41	2.52 ± 0.04	1.19 ± 0.06	1.07 ± 0.02	4.68 ± 0.04	4.52 ± 0.15
7.32S	0.18	1.38	0.23 ± 0.01	3.57 ± 0.17	3.08 ± 0.07	2.35 ± 0.10	1.15 ± 0.04	0.98 ± 0.02	4.54 ± 0.03	4.68 ± 0.17
9.76S	0.24	1.84	0.22 ± 0.01	3.16 ± 0.13	2.49 ± 0.18	2.14 ± 0.11	1.01 ± 0.07	0.84 ± 0.05	4.04 ± 0.03	4.00 ± 0.20
12.2S	0.31	2.30	0.21 ± 0.01	3.31 ± 0.28	2.42 ± 0.07	1.57 ± 0.05	1.00 ± 0.09	0.93 ± 0.02	4.01 ± 0.09	3.85 ± 0.18
14.64S	0.37	2.76	0.18 ± 0.01	1.99 ± 0.06	2.36 ± 0.19	1.57 ± 0.05	0.90 ± 0.12	0.86 ± 0.05	3.92 ± 0.10	4.43 ± 0.23
17.08S	0.43	3.22	0.20 ± 0.01	2.17 ± 0.19	2.10 ± 0.17	1.56 ± 0.04	0.95 ± 0.01	0.89 ± 0.01	3.52 ± 0.10	3.51 ± 0.25
2.44N	0.06	0.46	0.26 ± 0.01	3.61 ± 0.13	3.01 ± 0.07	2.41 ± 0.16	1.15 ± 0.03	1.10 ± 0.01	5.48 ± 0.01	5.77 ± 0.15
4.88N	0.12	0.92	0.22 ± 0.01	3.51 ± 0.16	3.06 ± 0.06	2.36 ± 0.17	1.15 ± 0.03	0.92 ± 0.03	4.88 ± 0.03	5.58 ± 0.16
7.32N	0.18	1.38	0.22 ± 0.01	3.23 ± 0.20	2.73 ± 0.11	2.48 ± 0.05	0.81 ± 0.01	1.02 ± 0.08	4.59 ± 0.05	5.28 ± 0.19
9.76N	0.24	1.84	0.21 ± 0.01	3.13 ± 0.09	2.68 ± 0.11	2.43 ± 0.13	1.04 ± 0.04	0.97 ± 0.02	4.27 ± 0.03	4.39 ± 0.14
12.2N	0.31	2.30	0.21 ± 0.01	3.01 ± 0.26	2.85 ± 0.04	2.21 ± 0.09	1.02 ± 0.04	0.90 ± 0.07	4.17 ± 0.09	4.77 ± 0.23
14.64N	0.37	2.76	0.18 ± 0.01	2.94 ± 0.21	2.81 ± 0.03	2.41 ± 0.16	0.92 ± 0.04	1.10 ± 0.13	4.10 ± 0.12	4.45 ± 0.23
17.08N	0.43	3.22	0.17 ± 0.01	2.60 ± 0.15	2.36 ± 0.16	1.77 ± 0.13	0.77 ± 0.02	0.99 ± 0.02	3.72 ± 0.11	4.37 ± 0.22
NGC 5903										
0.0	0.00	0.00	0.32 ± 0.01	3.59 ± 0.41	3.71 ± 0.01	2.17 ± 0.02	1.37 ± 0.01	1.22 ± 0.02	5.08 ± 0.28	7.70 ± 0.10
3.05 S	0.08	0.48	0.31 ± 0.01	3.85 ± 0.15	3.66 ± 0.03	2.37 ± 0.01	1.08 ± 0.03	1.17 ± 0.04	4.84 ± 0.06	5.57 ± 0.10
6.10 S	0.16	0.96	0.32 ± 0.01	4.30 ± 0.59	3.02 ± 0.02	2.33 ± 0.02	1.35 ± 0.02	1.19 ± 0.02	4.21 ± 0.05	5.24 ± 0.05
9.15 S	0.25	1.44	0.31 ± 0.01	3.68 ± 0.01	3.40 ± 0.03	2.69 ± 0.05	1.23 ± 0.02	1.23 ± 0.05	3.88 ± 0.11	4.73 ± 0.07
12.20S	0.33	1.92	0.27 ± 0.01	3.44 ± 0.11	3.47 ± 0.10	2.10 ± 0.03	1.41 ± 0.03	1.13 ± 0.04	3.97 ± 0.14	5.61 ± 0.04
15.25S	0.41	2.40	0.26 ± 0.02	2.94 ± 0.12	3.13 ± 0.05	2.09 ± 0.03	1.33 ± 0.01	1.13 ± 0.02	3.70 ± 0.10	5.34 ± 0.08
18.30S	0.49	2.88	0.29 ± 0.01	3.26 ± 0.14	3.02 ± 0.07	1.74 ± 0.12	1.30 ± 0.04	0.97 ± 0.03	3.31 ± 0.13	4.70 ± 0.08
24.40S	0.66	3.90	0.28 ± 0.02	2.63 ± 0.50	3.09 ± 0.04	2.08 ± 0.13	1.35 ± 0.07	0.95 ± 0.02	3.41 ± 0.15	5.50 ± 0.14
3.05 N	0.08	0.48	0.31 ± 0.01	3.45 ± 0.23	2.40 ± 0.06	1.78 ± 0.02	1.09 ± 0.03	1.09 ± 0.03	4.96 ± 0.10	7.14 ± 0.09
6.10 N	0.16	0.96	0.30 ± 0.01	3.39 ± 0.10	3.35 ± 0.04	2.16 ± 0.03	1.23 ± 0.02	0.91 ± 0.03	4.60 ± 0.07	6.54 ± 0.10
9.15 N	0.25	1.44	0.29 ± 0.02	3.62 ± 0.09	2.99 ± 0.05	2.60 ± 0.01	1.11 ± 0.02	0.86 ± 0.04	4.24 ± 0.08	6.08 ± 0.07
12.20N	0.33	1.92	0.25 ± 0.02	3.59 ± 0.10	3.03 ± 0.06	2.03 ± 0.03	0.95 ± 0.05	0.89 ± 0.02	4.09 ± 0.12	4.97 ± 0.09
15.25N	0.41	2.40	0.28 ± 0.02	3.45 ± 0.07	2.74 ± 0.03	2.49 ± 0.02	1.27 ± 0.03	0.91 ± 0.05	4.12 ± 0.15	5.99 ± 0.05
18.30N	0.49	2.88	0.27 ± 0.01	3.39 ± 0.09	3.37 ± 0.15	2.23 ± 0.03	1.34 ± 0.02	1.01 ± 0.02	3.76 ± 0.07	4.90 ± 0.08
24.40N	0.66	3.90	0.30 ± 0.02	3.28 ± 0.06	3.33 ± 0.06	1.98 ± 0.03	1.09 ± 0.02	0.72 ± 0.10	3.35 ± 0.08	5.48 ± 0.15

Table Notes. Note that EW of Mg_2 λ5176 is given in mag. Extraction area of all spectra of NGC 6868 is $3.66('')^2 \approx 0.12\,\mathrm{kpc}^2$. For NGC 5903 it is $4.57('')^2 \approx 0.12\,\mathrm{kpc}^2$, except for the outermost spectra, which is $9.15('')^2 \approx 0.25\,\mathrm{kpc}^2$. EWs are corrected by velocity dispersion and the errors are the standard deviation of three different measurements of the EW for each line.

work in the smaller galaxies. On the other hand, the lack of correlation between the Mg_2 gradient with mass above the $\sim 10^{11} M_\odot$ threshold might indicate that merging of smaller galaxies could be the dominant formation mechanism of massive galaxies.

To test where NGC 6868 and NGC 5903 occur in the $d\mathrm{Mg}_2/dlog\,r$ *vs.* galaxy mass, we compute their dynamical masses according to van Dokkum & Stanford (2003), with the data used in the present work. The results are $M_{NGC\,6868} = (3.2 \pm 0.1) \times 10^{11}\,M_\odot$ and $M_{NGC\,5903} = (1.8 \pm 0.1) \times 10^{11}\,M_\odot$, which agree, within the uncertainties, with the values computed by Carollo et al. (1993a). The average gradient values measured with our data are $(\mathrm{dMg_2/dlog\,r})_{\mathrm{NGC\,6868}} = -0.07 \pm 0.01\,\mathrm{mag}\,('')^{-1}$ and $(\mathrm{dMg_2/dlog\,r})_{\mathrm{NGC\,5903}} = -0.03 \pm 0.01\,\mathrm{mag}\,('')^{-1}$. Thus, according to the arguments developed by Carollo et al. (1993a), the present data are consistent with a merger origin for NGC 6868 and NGC 5903.

4 STELLAR POPULATION SYNTHESIS

The star formation history in a galaxy is a potential source of information not only on the age and metallicity distribution of the stellar population components. Dating the star-forming episodes may provide clues to better understand galaxy formation and evolution processes.

In what follows we investigate the star formation history of NGC 6868 and NGC 5903 by means of the stellar population synthesis method of Bica (1988). As population templates we use the synthetic star cluster spectra of Bruzual & Charlot (2003), built assuming a Salpeter (1955)

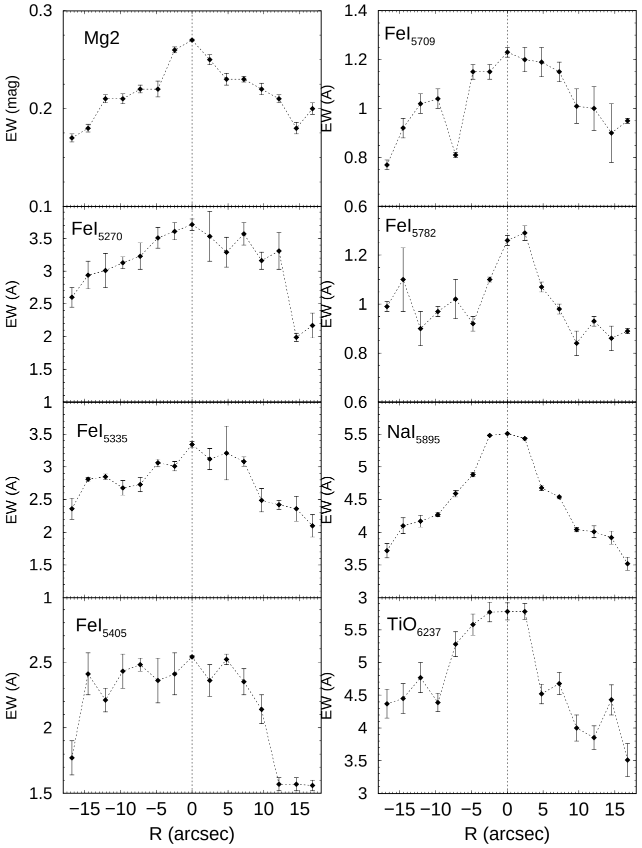

Figure 5. Spatial distribution of EWs measured in NGC 6868.

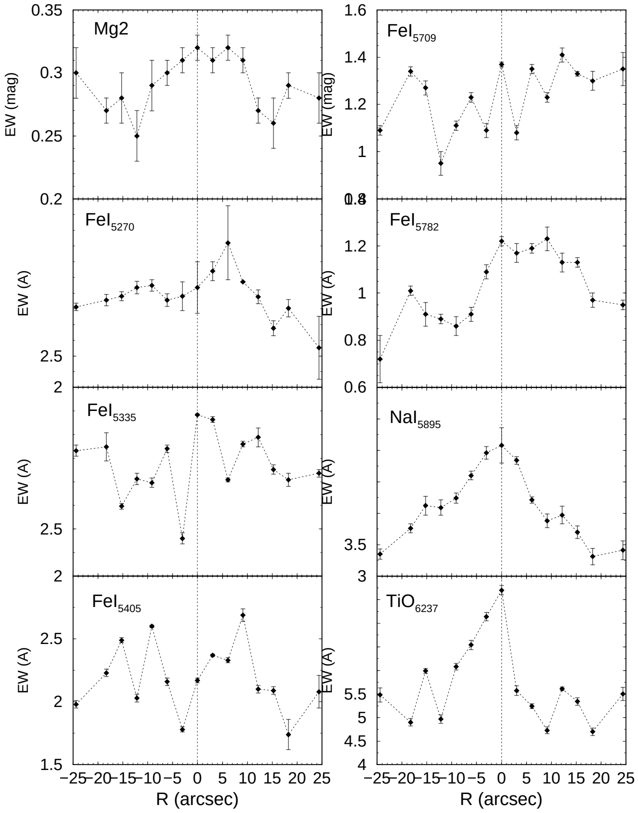

Figure 6. Same as Fig. 5 for the EWs of NGC 5903.

Table 3. Age and metallicity components

	$Z = 0.05$	$Z = 0.02$	$Z = 0.008$
13 Gyr	A1	A2	A3
5 Gyr	B1	B2	B3
1 Gyr		C2	

Initial Mass Function and masses in the range $0.6 \leqslant m \leqslant 120\,M_\odot$.

Before establishing the spectral base, we note that elliptical galaxies, in general, do not present recent star formation. Consequently, we only consider components older than 1 Gyr in the synthesis. The spectral base is made up of 7 components with ages of 1, 5 and 13 Gyr and metallicities $Z = 0.008,\ 0.02,$ and 0.05 (Table 3). These metallicities are taken as representative of the sub-solar, solar and above-solar ranges.

The stellar population synthesis provides directly the flux fractions (relative to the flux at λ5870) that each age and metallicity template contributes to the observed spectrum. The sum of the template spectra, according to the individual flux fractions, should be representative of the stellar population contribution to the observed spectrum. A full description of the method is in Rickes et al. (2004).

As a caveat we note that the observed spectra cover a relatively short spectral range and, thus, contain a reduced number of indices sensitive to age and metallicity that, in principle, could result in a small number of constraints for the synthesis, especially in terms of metallicity. However, the sum over metallicity shows that in the central regions of NGC 6868 and NGC 5903, the 13 Gyr population contributes with $70 \pm 16\%$ and $56 \pm 12\%$, respectively. The 5 Gyr population contributes with $28 \pm 15\%$ and $25 \pm 12\%$, respectively. These results suggest the presence of at least two populations of different ages in both galaxies, especially in the central parts. The stellar population synthesis results are summarized in Fig. 8, which shows $\sim 1\sigma$ differences in flux contribution between the 5 and 13 Gyr populations, along most of the galaxy's radial extent. Interestingly, the flux contribution of the 13 Gyr population in NGC 6868 increases towards the central region, while that of the 5 Gyr decreases, within uncertainties. Flux fractions distribute almost symmetrically with respect to the center of NGC 6868. In NGC 5903, both populations present almost uniform flux contributions, within uncertainties. The 1 Gyr population presents significant flux contributions only in the external regions ($|R| \gtrsim 2.3$ kpc) of NGC 6868, and in the central parts of NGC 5903.

We illustrate the stellar population synthesis in Fig. 9, where we superimpose on the central spectra of NGC 6868 and NGC 5903, the respective synthesized population spectra. The residuals in the model fit to NGC 6868 blueward of ∼ 5500 Å are probably due to bad calibration at the tail of the spectrum. The stellar population-subtracted spectrum of NGC 6868 present conspicuous emission lines, especially Hydrogen Balmer, [NII] and [SII]. NGC 5903, on the other hand, has no evidence of ionized gas.

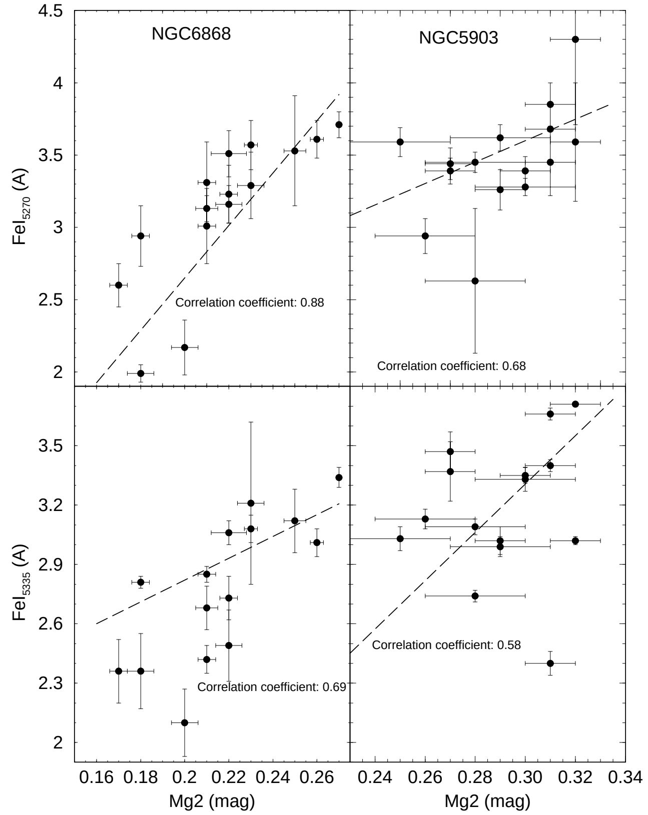

Figure 7. Correlations among selected Lick indices measured in NGC 6868 (left panels) and NGC 5903 (right panels).

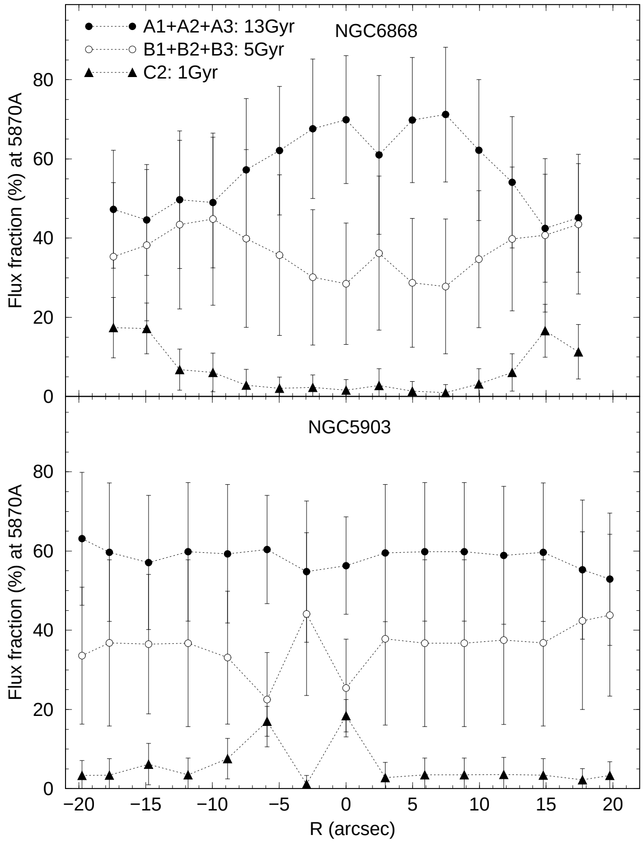

Figure 8. Flux-fraction contribution at 5870 Å of the stellar-population templates to the spectra of NGC 6868 (top panel) and NGC 5903 (bottom panel). In both cases the 5 and 13 Gyr components dominate the spectra, from the center to the external parts.

5 METALLICITY AND IONIZED GAS

5.1 Metallicity

Inferences on the metallicity of NGC 6868 and NGC 5903 can be made comparing the observed Lick indices of $\mathrm{Mg}_2\ \lambda 5176$, $FeI\,5270$ e $FeI\,5335$ with those derived from single-aged stellar population (SSP) models (Thomas et al. 2003, Buzzoni et al. 1992), that assume a Salpeter (1955) initial mass function and 10 Gyr of age.

Lick indices computed from SSP models for different metallicities and [α/Fe] ratios together with our data are shown in Fig. 10, with NGC 6868 in the top panel and NGC 5903 in the bottom. The central parts of NGC 6868 ($|R| \lesssim 0.5$ kpc) present a deficiency of alpha elements with respect to iron ($-0.3 \lesssim [\alpha/\mathrm{Fe}] \lesssim 0.0$) and an above-solar metallicity ($[Z/Z_\odot] \approx +0.3$. The external parts, on the other hand, present a higher, roughly uniform distribution of ratios ($[\alpha/\mathrm{Fe}] \approx +0.3$) and sub-solar metallicities ($[Z/Z_\odot] \approx -0.33$). The overabundance of the [α/Fe] ratios has been interpreted as a consequence of the chemical enrichment produced by type II supernovae with respect to type Ia ones (Idiart et al. 2003). Thus, differences measured in [α/Fe] imply different star-formation histories for the central and external regions of NGC 6868, which is consistent with the results derived from the stellar population synthesis (Sect. 4). A similar conclusion applies to NGC 5903 (bottom panel), since the central parts have metallicities in excess of $[Z/Z_\odot] \approx +0.35$ and $[\alpha/\mathrm{Fe}] \approx 0.0$, while the external parts have metallicities between solar and $[Z/Z_\odot] \approx +0.35$ and present an enhanced ratio $[\alpha/\mathrm{Fe}] \approx +0.3$.

5.2 Ionized gas

Emission gas has been recently detected in a large number of elliptical galaxies (Phillips et al. 1986). However, its origin and the nature of the ionization source have not yet been conclusively established. NGC 6868 presents conspicuous emission lines not only in the central region, but in spectra extracted up to R $\sim 17'' \sim 3.1$ kpc (Fig. 3). In what follows we investigate properties of the emission gas using fluxes of the lines $H\alpha$, $[NII]_{\lambda\lambda\,6548,6584}$, $[OI]_{\lambda\,6300}$ and $[SII]_{\lambda\lambda\,6717,6731}$, measured in the stellar population-free spectra, i.e., those resulting from the subtraction of the respective population templates (Sect. 4). The emission line fluxes were measured fitting Gaussian to the profiles.

Flux ratios with respect to $H\alpha$ are given in Tab. 4, and the spatial distribution of the measured ratios $\frac{[OI]}{H\alpha}$, $\frac{[NII]}{H\alpha}$ and $\frac{[SII]}{H\alpha}$ are shown in the left panels of Fig. 11.

Assuming case B recombination, the number of ionizing photons can be computed from H_α luminosity using the equation $Q(H) = \frac{L_{H\alpha}}{h\nu_\alpha}\frac{\alpha_B(H^0,T)}{\alpha_{H\alpha}(H^0,T)}$ (Osterbrock 1989), where $\alpha_B\,(H^0,T)$ is the total recombination coefficient, and $\alpha_{H\alpha}\,(H^0,T)$ is the recombination coefficient for Hα. Values

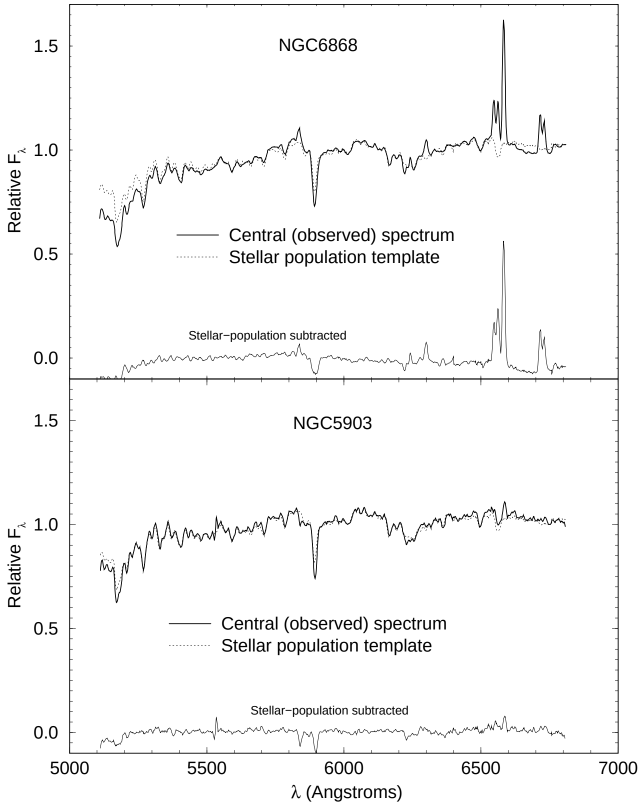

Figure 9. Stellar population synthesis of NGC 6868 (top panel) and NGC 5903 (bottom panel). Notice that the subtraction of the stellar population enhanced $H\alpha$ in emission in NGC 6868.

Table 4. Emission line parameters of NGC 6868

$R('')$ (1)	$H\alpha$ (2)	$\frac{[NII]}{H\alpha}$ (3)	$\frac{[SII]}{H\alpha}$ (4)	$\frac{[OI]}{H\alpha}$ (5)
0.00	3.36 ± 0.08	2.81 ± 0.21	1.23 ± 0.10	0.51 ± 0.04
2.44S	3.39 ± 0.10	2.90 ± 0.91	1.18 ± 0.12	0.33 ± 0.04
4.88S	1.81 ± 0.11	2.46 ± 0.21	0.92 ± 0.11	0.51 ± 0.07
7.32S	1.20 ± 0.18	2.36 ± 0.36	0.88 ± 0.40	0.92 ± 0.17
9.76S	0.82 ± 0.21	2.36 ± 0.61	1.20 ± 0.31	1.23 ± 0.34
2.44N	3.83 ± 0.13	2.92 ± 0.32	1.32 ± 0.11	0.29 ± 0.03
4.88N	2.86 ± 0.10	2.65 ± 0.22	1.30 ± 0.12	0.26 ± 0.04
7.32N	2.34 ± 0.13	2.87 ± 0.64	1.25 ± 0.10	0.19 ± 0.05
9.76N	2.08 ± 0.16	3.11 ± 0.42	1.39 ± 0.11	0.35 ± 0.06
12.20N	1.49 ± 0.13	2.88 ± 0.33	1.47 ± 0.41	0.56 ± 0.11
14.64N	1.39 ± 0.18	2.56 ± 0.57	1.23 ± 0.17	–
17.08N	1.06 ± 0.20	2.43 ± 0.48	1.20 ± 0.23	–

Table Notes. $H\alpha$ flux in col. 2 is given in $10^{-15}\,\mathrm{erg\,s^{-1}\,cm^{-2}}$.

of $Q(H)$ and $L_{H\alpha}$ for NGC 6868 are given in Tab. 5, and their spatial distributions are shown in panels (d) and (e) of Fig. 11.

Fig. 11 also shows that in all extracted spectra of NGC 6868, the ratio $\frac{[NII]_{\lambda 6584}}{H\alpha}$ is larger than 1 and $\frac{[SII]_{\lambda 6731}}{H\alpha}$ is smaller than 1, within uncertainties.

With the above facts in mind we consider three possible scenarios to infer the nature of the ionization source in NGC 6868. They involve the presence of star clusters, post-AGB stars and an AGN.

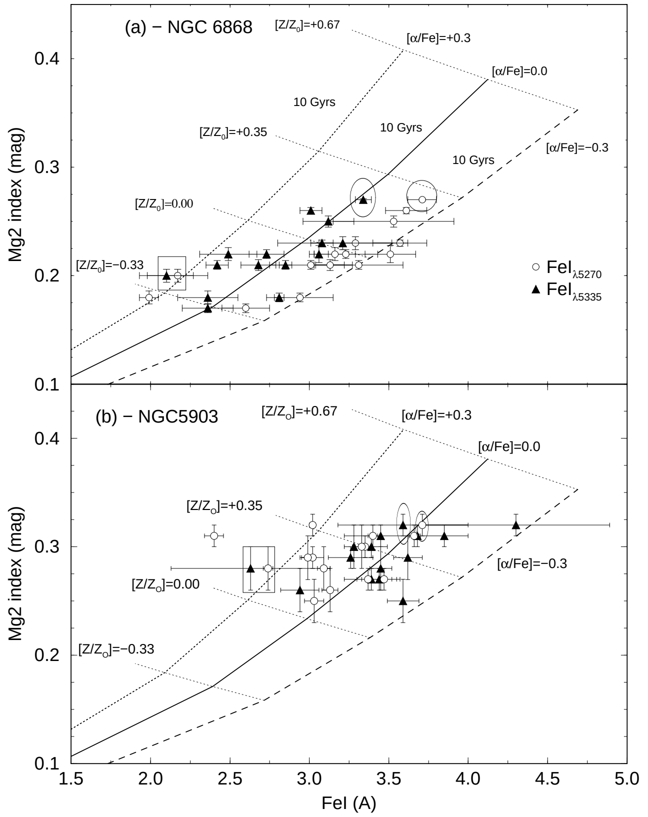

Figure 10. Selected Lick indices measured in NGC 6868 (top panel) and NGC 5903 (bottom panel) are compared to those computed from SSP models for a range of metallicity and [α/Fe] ratios. Ellipses and boxes indicate the central and external regions respectively.

Table 5. $H\alpha$ luminosity and number of ionizing photons in NGC 6868

R $('')$	$L_{H\alpha}$ $(10^{38}\,\mathrm{erg\,s^{-1}})$	$Q(H)$ $(10^{51}\,\mathrm{s^{-1}})$
0.00	5.8 ± 1.2	2.6 ± 0.5
2.44S	5.9 ± 1.2	2.6 ± 0.5
4.88S	3.1 ± 0.6	1.4 ± 0.3
7.32S	2.1 ± 0.4	0.9 ± 0.2
9.76S	1.4 ± 0.3	0.6 ± 0.1
2.44N	6.6 ± 1.3	2.9 ± 0.6
4.88N	4.9 ± 1.0	2.2 ± 0.4
7.32N	4.0 ± 0.8	1.8 ± 0.4
9.76N	3.6 ± 0.7	1.6 ± 0.3
12.20N	2.6 ± 0.5	1.1 ± 0.2
14.64N	2.4 ± 0.3	1.1 ± 0.1
17.08N	1.8 ± 0.4	0.8 ± 0.2

Table Notes. $H\alpha$ luminosity and number of ionizing photons computed for the extractions given in col. 1 of NGC 6868.

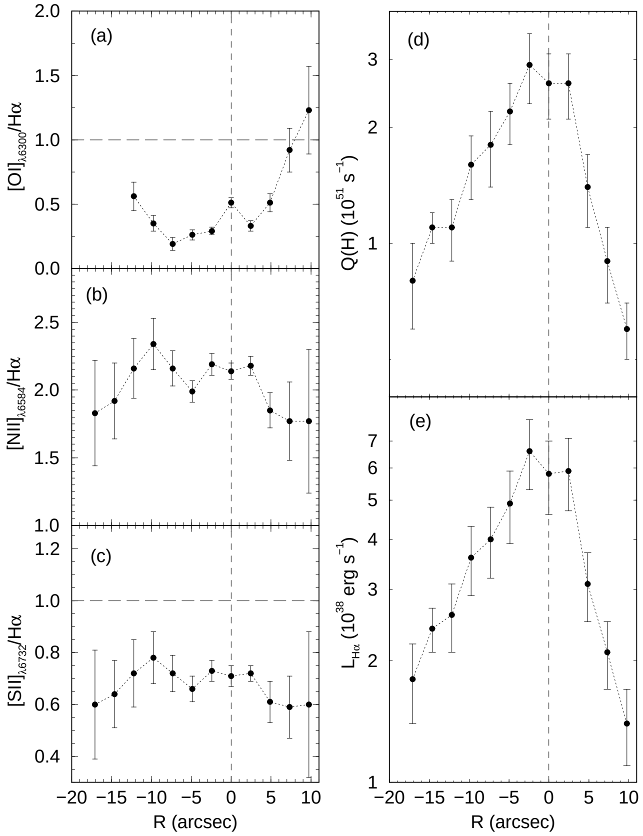

Figure 11. Spatial variation of the ratios $\frac{[OI]_{\lambda\,6300}}{H\alpha}$ (panel a), $\frac{[NII]_{\lambda6584}}{H\alpha}$ (b) and $\frac{[SII]_{\lambda6731}}{H\alpha}$ (c). Panels (d) and (e) show the spatial distribution of the number of ionization photons and $H\alpha$ luminosity, respectively. The dashed line in panels (a) and (c) discriminates between different ionizing sources (Sect. 5.2.2).

5.2.1 Star cluster

To test this hypothesis we build a star cluster that produces a total number of ionizing photons of the order of $10^{51}\,\mathrm{s}^{-1}$ following Salpeter (1955) initial mass function, $\phi(m) \propto m^{-(1+\chi)}$, with $\chi = 1.35$, considering stars in the mass range $0.1 - 100\,M_\odot$. For the relation of number of ionizing photons (N_{Ly}) with stellar mass we use the library of stellar atmospheres of Kurucz (1979). In cols. 2 and 3 of Table 6 we provide N_{Ly} for ionizing stars in the mass range $10 - 30\,M_\odot$. In this mass range, the number of ionizing photons can be related to stellar mass by the approximation $N_{Ly}(m) \approx 3.9 \times 10^{39} \left(\frac{m}{M_\odot}\right)^{5.9}\,\mathrm{s}^{-1}$. Thus, the total number of ionizing photons can be computed from $\int_{10}^{30} N_{Ly}(m)\phi(m)dm$.

The resulting distribution of stars in terms of spectral type of the hypothetical ionizing star cluster is given in col. 4 of Tab. 6 for representative spectral types. Because of the large number of O5 stars, such a star cluster would be very young, luminous and have a mass of $\sim 10^6\,M_\odot$.

We conclude that ionization by such a massive star cluster can be ruled out, because with more than 200 O5 stars it should be bright enough to be easily identified in images. Besides, its flux contribution to the observed spectra should be conspicuously detected by the stellar population synthesis (Sect. 4).

Table 6. Hypothetical ionizing star cluster

Spectral type (1)	m ($M_\odot$) (2)	N_{Ly} ($10^{48}\,\mathrm{s}^{-1}$) (3)	Number of stars (4)
O5	30	2.00	226
	22	0.25	470
B0	17	0.082	860
	15	0.043	1154
	13	0.015	1616
	10	0.0021	2993

5.2.2 Post-AGB stars

Since a typical Post-AGB star emits $\sim 10^{47}\,\mathrm{s}^{-1}$ (Binette 1994), about 10^4 such stars would be necessary to produce the amount of ionizing photons measured in each extracted region (Tab. 6). All spectra of NGC 6868 were extracted from regions with an area of $\approx 0.19\,\mathrm{kpc}^2$. This implies a projected number density of Post-AGB stars of $\sim 8\times10^4\,\mathrm{kpc}^{-2}$ scattered throughout the $R \approx 3.3\,\mathrm{kpc}$ central region. Such a density is not absurd (Binette 1994), however, Post-AGB star ionization models for a variety of ionization parameters predict that the intensity ratio $[OI]_{\lambda6300}/H\alpha$ should be smaller than unity, while those of $[SII]_{\lambda6731}/H\alpha$ and $[NII]_{\lambda6584}/H\alpha$ should be smaller than ≈ 1.5. The first two conditions are met by the measurements of NGC 6868, but the ratios $[NII]_{\lambda6584}/H\alpha$ are all above 1.5 (Fig 11).

The presence of a significant number of post-AGB stars in early-type galaxies produces a conspicuous excess in the UV flux, e.g. Bica et al. (1996). NGC 6868 is included in the galaxies investigated by Bonatto et al. (1996), among those with a flat UV spectrum, which is consistent with the above arguments against a numerous population of post-AGB stars in this galaxy.

5.2.3 Active Nucleus

To test this hypothesis we build diagnostic-diagrams involving the ratios $[NII]_{\lambda6584}/H\alpha$, $[OI]_{\lambda6300}/H\alpha$ and $[SII]_{\lambda6717,31}/H\alpha$, using as comparison the values measured in a sample if nearby galaxies with low luminosity ($\mathrm{L_{H\alpha}} < 2\times10^{39}\,\mathrm{erg\,s^{-1}}$) active nucleus (Ho et al. 1997). Here we use the galaxies in Ho et al. (1997) sample with unambiguous classification as LINER in spiral, LINER in elliptical, Seyfert or Starburst. The restricted sample amounts to 128 galaxies.

The results are shown in Fig. 12, where in both panels we see that the values measured in NGC 6868 consistently fall in the locus occupied predominantly by LINERs.

These results, together with those of the stellar population synthesis, suggest that the main source of gas ionization in NGC 6868 is non-thermal. However, as a caveat we note that shocks can also produce emission-line ratios similar to those measured in NGC 6868. In this sense, the ratios $[NII]_{\lambda6584}/H\alpha$ and $[SII]_{\lambda6717,31}/H\alpha$ alone cannot discriminate between the AGN and shocks as the ionization source. Indeed, Storchi-Bergmann et al. (1996) show that a

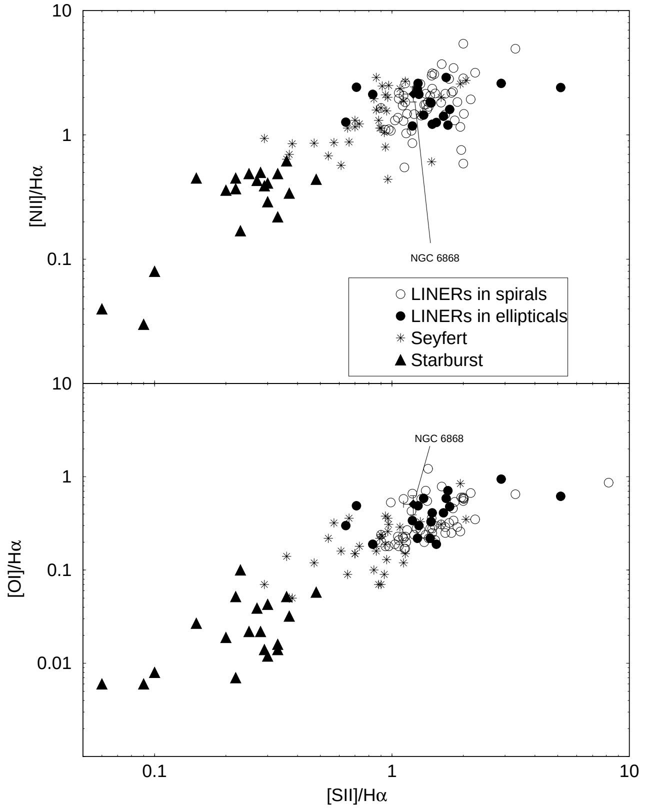

Figure 12. Emission-line diagnostic diagrams with a subsample of the galaxies in Ho et al. (1997) plotted as comparison. The locus of NGC 6868 in both diagrams is consistent with that of LINERs.

low-luminosity AGN cannot ionize gas up to distances of $\sim$ 3.5 kpc. Besides, they suggest that ionization in the external region is produced by shocks, which accounts for the constancy of the $[NII]_{\lambda6584}/H\alpha$ and $[SII]_{\lambda6717,31}/H\alpha$ ratios.

6 DISCUSSION AND CONCLUDING REMARKS

The stellar population, metallicity distribution and ionized gas in NGC 6868 and NGC 5903 have been investigated in this paper by means of long-slit spectroscopy and stellar population synthesis. Lick indices of both galaxies consistently present a negative gradient that indicates an over-abundance of Fe, Mg, Na and TiO in the central parts with respect to the external regions. We found that Mg_2 correlates both with FeI$_{\lambda5270}$ and FeI$_{\lambda5335}$, which suggests that these elements probably underwent the same enrichment process in NGC 6868. However, in NGC 5903 only a marginal correlation of Mg_2 and FeI$_{\lambda5270}$ occurs.

Galaxy mass and the Mg_2 gradient computed in the present work are consistent with previous results that suggest that NGC 6868 and NGC 5903 were formed by merger events. In addition, the stellar population synthesis clearly shows the presence of at least two populations of different ages in both galaxies. Particularly in the central regions of NGC 6868 and NGC 5903, the 13 Gyr population contributes with $70 \pm 16\%$ and $56 \pm 12\%$, respectively. The 5 Gyr population contributes with $28 \pm 15\%$ and $25 \pm 12\%$, respectively in flux fraction at 5870 Å.

The central regions of NGC 6868 and NGC 5903 present a deficiency of alpha elements with respect to the external parts, which suggests different star-formation histories in both regions. With respect to the metallicity, the central regions of both galaxies have higher $[Z/Z_{\odot}]$ values than the external parts. The range in metallicity spanned by the sampled regions of NGC 6868 appears to be larger than in NGC 5903.

Concerning the ionized gas in NGC 6868, the ratios $[NII]_{\lambda6584}/H\alpha$, $[OI]_{\lambda6300}/H\alpha$ and $[SII]_{\lambda6717,31}/H\alpha$ consistently suggest the presence of a LINER at the galaxy center. These results, together with the stellar population synthesis, suggest that the main source of gas ionization in NGC 6868 is non-thermal, produced by a low-luminosity active nucleus, probably with some contribution of shocks to explain ionization at distances of $\sim$ 3.5 kpc from the nucleus.

ACKNOWLEDGMENTS

We thank the anonymous referee for helpful suggestions. We acknowledge the Brazilian agency CNPq for partial support of this work. This research has made use of the NASA/IPAC Extragalactic Database (NED) which is operated by the Jet Propulsion Laboratory, California Institute of Technology, under contract with the National Aeronautics and Space Administration.

REFERENCES

Arimoto, N., YosHII, Y. 1987, A&A, 23, 38

Bica, E. 1988, A&A, 195, 79

Bica, E., Bonatto, C., Pastoriza, M.G. & Alloin, D. 1996, A&A, 313, 405

Bica, E., Arimoto, N. & Alloin, D. 1988, A&A, 202, 8

Binette, L. Magris, C. G. Stasinska, G. Bruzual, A.G., 1994, A&A, 292, 13

Bonatto, C., Bica, E., Pastoriza, M.G. & Alloin, D., 1996, A&A, 118, 89

Bruzual, G., Charlot, S. 2003, MNRAS, 344, 1000

Burkert, A.; Naab, T. 2000, A&AS, 23, 1497

Buzzoni, A.; Mantegazza, L., Gariboldi, G. 1994, ApJ., 107, 513

Caon, N., Macchetto, D., Pastoriza, M. 2000, ApJS, 127, 39

Cardelli, J. A., Clayton, G. C. & Mathis, J. S. 1989, ApJ, 345, 245

Carollo, C. M., Danziger, I.J., Buson, L. 1993a, MNRAS, 265, 553

Carollo, C. M., Danziger, I.J., Buson, L. 1993b, MNRAS, 553, 580

Carollo, C. M., Danziger, I.J. 1994a, MNRAS, 270, 523

Carollo, C. M., Danziger, I.J. 1994b, MNRAS, 270, 743

Chiosi, C. & Carraro, G. 2002, MNRAS, 335, 335

Davies, R.L., Burstein, D., Dressler, A., Faber, S.M., Lynden-Bell, D., Terlevich, R., Wegner, G. 1987, ApJS, 64, 581

Davies, R.L., Sadler, E.M., Peletier, R.F. 1993, MNRAS, 262, 650

Davies, R.L., Sadler, E.M., Peletier, R.F. 1993, MNRAS, 650, 680

de Vaucouleurs, G., de Vaucouleurs, A., Corwin, H. G., Jr., Buta, R. J., Paturel, G., Fouque, P., 1991.

Faber, S. M., Friel, E. D., Burstein, D., Gaskell, C. M. 1985, ApJS, 57, 711

Ferrari, F., Pastoriza, M. G., Macchetto, F., Caon, N. 1999, A&A, 136, 269

Ferrari, F.; Pastoriza, M. G.; Macchetto, F. D.; Bonatto, C.; Panagia, N.; Sparks, W. B. 2002, A&A, 389, 355

Ho, L.C., Filippenko, A.V., Sargent, W.L.W., 1997, APJ, 112, 315

Idiart, T.P., Michard, R. & de Freitas Pacheco, J.A., 2003, A&A, 398, 949

Kurucz, R. L. 1979, ApJS, 40, 1

Macchetto, F., Pastoriza, M., Caon, N., Sparks, W.B., Giavalisco, M., Bender, R., Capaccioli, M. 1996, A&A, 120, 463

Maia, M. A. G., Da Costa, L. N. Latham, D. W., 1989, AJSS, 69, 809

Ogando, R.L.C., Maia, M.A.G., Chiappini, C., Pellegrini, P.S., Schiavon, R.P., da Costa, L.N. 2005, ApJ, 61, 64

O'Sullivan, E., Forbes, D. A., Ponman, T. J., 2001, MNRAS, 328, 461

Osterbrock, D. E., 1989, in "Astrophisics of Gaseous Nebulae and Active Galactic Nuclei", University Science Books

Phillips, M. M., Jenkins, C. R., Dopita, M. A., Sadler, E. M., Binette, L., 1986, ApJ, 91, 1062

Rickes, M. G,; Pastoriza, M.G., Bonato, C., 2004, 419, 449

Salpeter, E.F., 1979, ApJ, 121, 161

Savage, A., Wright, A. E., Bolton, J. G. 1977, AuJPAS, 44, 1

Schweizer, F., Seitzer, P., Faber, S. M.; Burstein, D., Dalle Ore, C. M., Gonzalez, J. J. 1990, ApJ, 364, 33

Sparks, W.B., Wall, J.V., Thorne, D.J., Jorden, P.R, van Breda, I.G., Rudd, P.J., Jorgensen, H.E., 1985, MNRAS, 217, 89

van Dokkum, P., Standord, S. A., 2003, ApJ, 285, 79

Storchi-Bergmann, Thaisa; Wilson, Andrew S.; Baldwin, Jack A., 1996, APJ, 460, 252

Thomas, D., Maraston, C., Bender, R., 2003, MNRAS, 339, 897

Worthey, G. 1994, ApJS, 95, 107

Worthey, G.; Faber, S. M.; Gonzáles, J. J . 1992, ApJS, 398, 69

Zeilinger, W.W., Pizzella, A., Amico, P., Bertin, G., Bertola, F., Buson, L. M., Danziger, I. J., Dejonghe, H., Sadler, E. M., Saglia, R. P., de Zeeuw, P. T., 1996, A&AS, 120, 257